

Separation of Powers in Federated Learning

Pau-Chen Cheng
IBM Research
New York, USA
pau@us.ibm.com

Kevin Eykholt
IBM Research
New York, USA
kheykholt@ibm.com

Zhongshu Gu*
IBM Research
New York, USA
zgu@us.ibm.com

Hani Jamjoom
IBM Research
New York, USA
jamjoom@us.ibm.com

K. R. Jayaram*
IBM Research
New York, USA
jayaramkr@us.ibm.com

Enriquillo Valdez
IBM Research
New York, USA
rvaldez@us.ibm.com

Ashish Verma
IBM Research
New York, USA
ashish.verma1@ibm.com

ABSTRACT

Federated Learning (FL) enables collaborative training among mutually distrusting parties. Model updates, rather than training data, are concentrated and fused in a central aggregation server. A key security challenge in FL is that an untrustworthy or compromised aggregation process might lead to unforeseeable information leakage. This challenge is especially acute due to recently demonstrated attacks that have reconstructed large fractions of training data from ostensibly “sanitized” model updates.

In this paper, we introduce TRUDA, a new cross-silo FL system, employing a trustworthy and decentralized aggregation architecture to break down information concentration with regard to a single aggregator. Based on the unique computational properties of model-fusion algorithms, all exchanged model updates in TRUDA are disassembled at the parameter-granularity and re-stitched to random partitions designated for multiple TEE-protected aggregators. Thus, each aggregator only has a fragmentary and shuffled view of model updates and is oblivious to the model architecture. Our new security mechanisms can fundamentally mitigate training data reconstruction attacks, while still preserving the final accuracy of trained models and keeping performance overheads low.

1 INTRODUCTION

Federated Learning (FL) [37] provides a collaborative training mechanism, which allows multiple parties to build a joint machine learning (ML) model. FL allows parties to retain private data within their controlled domains. Only model updates are shared to a central aggregation server. The security setting of FL is especially attractive for mutually distrusting/competing training participants as well as holders of sensitive data (e.g., health and financial data) seeking to preserve data privacy.

FL is typically deployed in two scenarios: *cross-device* and *cross-silo* [26]. The *cross-device* scenario involves a large number of parties (> 1000), but each party has a small number of data items, constrained compute capability, and limited energy reserve (e.g., mobile phones or IoT devices). They are highly unreliable and are expected to drop and join frequently. Examples include a large organization learning from data stored on employees’ devices and a device manufacturer training a model from private data located on millions of its devices (e.g., Google Gboard [6]). A *trusted authority*, which performs aggregation and orchestrates training, is typically present in a *cross-device* scenario. Contrarily, in the *cross-silo* scenario, the

number of parties is small, but each party has extensive compute capabilities (with stable access to electric power and/or equipped with hardware ML accelerators) and large amounts of data. The parties have reliable participation throughout the entire FL training life-cycle, but are more susceptible to sensitive data leakage. Examples include multiple hospitals collaborating to train a tumor detection model on radiographs, multiple banks collaborating to train a credit card fraud detection model, etc. In *cross-silo* scenarios, there exists *no presumed central trusted authority*. All parties involved in the training are *equal* collaborators. The deployments often involve hosting aggregation in public clouds, or alternatively one of the parties acting as, and providing infrastructure for aggregation. In this paper, we focus on examining the trustworthiness of collaborative learning in *cross-silo* scenarios.

There was a *misconception* that the exchanged model updates in FL communications would contain far less, if any, information about the raw training data. Thus, sharing model updates was considered to be “privacy-preserving.” However, although not easily discernible, training data information is still embedded in the model updates. Recent research [12, 39, 62, 63, 67] has demonstrated the feasibility and ease of inferring private attributes and reconstructing large fractions of training data by exploiting model updates, thereby challenging the privacy promises of FL in the presence of honest-but-curious aggregation servers. Furthermore, since aggregation often runs on untrustworthy cloud or third-party infrastructures in the *cross-silo* scenarios, we need to re-examine the trust model and system architecture of current FL frameworks under this new attack scenario.

Existing solutions that reinforce FL privacy include (1) Differential Privacy (DP) based aggregation through the addition of statistical noise to model updates [3, 13, 38, 50, 53], and (2) using Secure Multi-Party Computation (SMC) or Homomorphic Encryption (HE) [1, 7, 17, 41] for aggregation. Both techniques have several drawbacks. The former often significantly decreases the accuracy of the trained model and needs careful hyper-parameter tuning to minimize accuracy loss. The latter is computationally expensive, with aggregation overheads significantly outpacing training time [25].

Our work is motivated by the following key insights: (I) The *concentration* of model updates in a central FL aggregator discloses significantly more information than what is required by the aggregation/model-fusion algorithms. This gap, indeed, facilitates data reconstruction attacks if the central aggregator is compromised. (II) FL model-fusion algorithms are *bijective* and only

*Corresponding authors.

involve *coordinate-wise* arithmetic operations across model updates. Partitioning and (internally) shuffling model updates do not change the fusion results, thus having no impact on the final model accuracy and convergence rate compared to traditional (insecure) FL training. We only need to ensure that the local transformation of model updates is deterministic, reversible, and synchronized across parties. From the attacker’s point of view, partitioning and shuffling operations fully disrupt the completeness and data-order of model updates, which are indispensable for reconstructing training data. (III) Trusted Execution Environments (TEEs) can help establish confidential and remote-attestable execution entities on untrustworthy servers. The missing link is how to authenticate and connect all individual entities to bootstrap trust in a distributed FL ecosystem.

In this paper, we introduce TRUDA¹, a new cross-silo FL system for deep neural network (DNN) training. In TRUDA, we employ multiple, rather than one, TEE-protected decentralized aggregators. All model updates are disassembled at the parameter-granularity and re-stitched (with shuffling) to random partitions designated for different aggregators. Thus, each aggregator only has a fragmentary and out-of-order view of each model update and is oblivious to the model architecture. This new system architecture can fundamentally minimize the information leakage surface for data reconstruction attacks, but with no utility loss regarding model aggregation. We have implemented three composable security-reinforced mechanisms in TRUDA:

Trustworthy Aggregation. We leverage TEEs to protect the model fusion process. Every aggregator runs within an encrypted virtual machine (EVM) via AMD Secure Encrypted Virtualization (SEV). All in-memory data are kept encrypted at runtime during model aggregation. To bootstrap trust between parties and aggregators, we design a two-phase attestation protocol and develop a series of tools for integrating/automating confidential computing in FL. Each party can authenticate trustworthy aggregators before participating in FL training. End-to-end secure channels, from the parties to the EVMs, are established after attestation to protect model updates in transit.

Decentralized Aggregation. Decentralization was primarily investigated in distributed learning [2, 6, 30, 31, 58] as a load balancing technique for enhancing system performance; model updates were distributed among aggregator replicas with each update assigned to a single replica and each replica seeing the entire model update from a party. This still provided a fertile ground for data reconstruction attacks on the aggregator side. Instead, we choose a security-centric decentralization strategy by employing fine-grained model partitioning to break down information concentration. We launch multiple aggregators within TEEs. Each aggregator only receives a fraction of model update with no knowledge of the whole model architecture. The parties share a model-mapper at parameter-granularity for disassembling and re-stitching a local model update into disjoint partitions, which are dispatched to corresponding aggregators. Furthermore, users can deploy multiple aggregators to physical servers at different geo-locations and potentially with diversified TEEs, e.g., Intel SGX [36]/ TDX [24], IBM PEF [19], etc. Thus, we can prevent model aggregation from becoming a single point of

failure (i.e., leaking entire and intact model updates) under security attacks.

Shuffled Aggregation. Based on the bijective property of model-fusion algorithms, we allow parties to permute the fragmentary model updates to further obfuscate the information sent to each aggregator. The permutation changes dynamically at each training round. This strategy guarantees that even if *all* decentralized aggregators are breached, adversaries will still require the permutation key to be able to decipher the correct ordering of the model updates and reconstruct the training data.

In our security analysis, we reproduced three state-of-the-art training data reconstruction attacks [12, 63, 67] and plugged in TRUDA for generating the model updates. Our experiments demonstrate that TRUDA renders all the attacks ineffective for reconstructing local training data. In our performance evaluation, we measured the accuracy/loss and latency for training deep learning models on the datasets, *MNIST*, *CIFAR-10*, and *RVL-CDIP*[18], with a spectrum of aggregation algorithms and FL configurations. We demonstrate that TRUDA can achieve the same level of accuracy/loss and converge at the same rate, with minimal performance overheads compared to the traditional federated learning platform as baseline.

2 THREAT MODEL

Our threat model assumes honest-but-curious aggregation servers, which are susceptible to compromise. Adversaries attempt to attack aggregators and inspect model updates uploaded from parties. Their purpose is to reconstruct training data of parties that participate in the FL training. We consider that the parties involved in FL training are benign and will not collude with other parties to share training data. This threat model is the same as in the FL data reconstruction attacks [12, 62, 63, 67].

In addition, our threat model is consistent with the one assumed in AMD SEV. We consider that parties involved in FL trust AMD System-on-Chip (SoC) and the EVMs launched to hold the model aggregation workloads. Adversaries can not only execute user-level code on the aggregator’s hosting machines, but can also execute malicious code at the level of privileged system software, e.g., operating system (OS), hypervisor, BIOS, etc. The attacker may also have physical access to the DRAM of hosting machines. Our current FL system implementation is based on the 1st-generation SEV [28] on EPYC 7642 (ROME) microprocessor, which is the latest release available on the market. Based on the white papers, the following SEV generations, i.e., SEV-ES [27] and SEV-SNP [48], will include confidentiality protection for virtual machine (VM) register state and integrity protection to defend against memory corruption, aliasing, remapping, and replay attacks. Our threat model can be elevated to follow the stronger isolation protection of future SEV releases.

Recently, some research efforts [8, 32, 33, 59, 60] focus on discovering potential vulnerabilities of SEV. In this paper, we do not intend to address these problems and consider they will be fixed with the AMD’s firmware updates or in the upcoming SEV-SNP release. However, *even if EVMs are breached*, our design of decentralized and shuffled aggregation of model updates will still be effective at preventing adversaries from reconstructing training data.

¹TRUDA stands for TRUstworthy and Decentralized Aggregation

3 BACKGROUND

This section provides relevant information on common FL aggregation algorithms, data reconstruction attacks, computational properties of FL aggregation algorithms and AMD SEV that are leveraged by TRUDA.

3.1 Aggregation Algorithms for DNN Training

Federated Stochastic Gradient Descent (FedSGD) [50] and Federated Averaging (FedAvg) [37] are the most common FL aggregation algorithms for DNN training, employing iterative merging and synchronizing model updates. Other DNN aggregation methods, e.g., Byzantine-robust fusions like *Coordinate Median* [61]/*Krum* [5] and *Paillier crypto fusion* [1, 34, 53], have the similar algorithmic structure with additional security enhancements. TRUDA can support all of them with no change. Here we describe the algorithms of *FedSGD* and *FedAvg* in detail.

We use θ to denote model parameters and L for the loss function. Each party has its own training data/label pairs (x_i, y_i) . The parties choose to share the gradients $\nabla_{\theta} L_{\theta}(x_i, y_i)$ for a data batch to the aggregator. The aggregator computes the gradient sum of all parties and lets the parties synchronize their model parameters: $\theta \leftarrow \theta - \eta \sum_{i=1}^N \nabla_{\theta} L_{\theta}(x_i, y_i)$. This aggregation algorithm is called *FedSGD*. Alternatively, the parties can also train for several epochs locally and upload the model parameters: $\theta^i \leftarrow \theta^i - \eta \nabla_{\theta^i} L_{\theta^i}(x_i, y_i)$ to the aggregator. The aggregator computes the weighted average of model parameters $\theta \leftarrow \sum_{i=1}^N \frac{n_i}{n} \theta^i$, where n_i is the size of training data on party i and n is the sum of all n_i . Then, the aggregator sends the aggregated model parameters back to the parties for synchronization. This aggregation algorithm is called *FedAvg*. *FedAvg* and *FedSGD* are equivalent if we train only one batch of data in a single FL training round and synchronize model parameters, as gradients can be computed from the difference of two successive model parameter uploads. As *FedAvg* allows parties to batch multiple SGD iterations before synchronizing updates, it would be more challenging for data reconstruction attacks to succeed.

3.2 Data Reconstruction Attacks

Exchanging model updates in *FedAvg* and *FedSGD* was considered privacy-preserving as original training data were not directly included in communications. However, recent attacks, e.g., Deep Leakage from Gradients (DLG) [67], Improved Deep Leakage from Gradients (iDLG) [63], and Inverting Gradients (IG) [12], have demonstrated that it is possible to derive training data samples from the model updates.

In DLG [67], the attack reconstructed a training sample x based on the shared gradient updates. The attack randomly initialized a dummy input x' and label y' , which were fed into the model in order to compute the loss gradients. Then, the attack used an L-BGFS solver to minimize the following cost function in order to reconstruct x :

$$\operatorname{argmin}_{x', y'} \|\nabla_{\theta} L_{\theta}(x', y') - \nabla_{\theta} L_{\theta}(x, y)\|^2$$

As the differentiation requires second order derivatives, the attack only works on models that are twice differentiable. Zhao et al. [63] found that although the DLG attack was effective, the reconstructions and labels generated after optimization were sometimes of low

quality and incorrect respectively. In their iDLG attack, the authors demonstrated that the signs of the loss gradients with respect to the correct label are always opposite to the signs of the other labels. Thus, the ground truth labels can be inferred based on the model updates, which improve reconstruction quality.

IG [12] makes two major modifications to DLG and iDLG. First, the authors asserted that it is not the magnitudes of the gradients that are important, but rather the directions of the gradients. Based on this reasoning, they used a cosine distance cost function, which encouraged the attack to find reconstructions that resulted in the same changes in gradients' directions. Their new cost function is:

$$\operatorname{argmin}_{x' \in [0,1]} 1 - \frac{\langle \nabla_{\theta} L_{\theta}(x', y), \nabla_{\theta} L_{\theta}(x, y) \rangle}{\|\nabla_{\theta} L_{\theta}(x', y)\| \|\nabla_{\theta} L_{\theta}(x, y)\|} + \alpha TV(x')$$

They also (i) constrained their search space to $[0, 1]$, (ii) added total variation as an image prior, and (iii) minimized their cost function based on the signs of the loss gradients and the ADAM optimizer. This modification was inspired by adversarial attacks on DNNs, which used a similar technique to generate adversarial inputs [51].

3.3 Bijectivity of Aggregation Algorithms

Most DNNs aggregation algorithms (e.g., *FedAvg*, *FedSGD*, *Krum*, *Coordinate Median*, *Paillier crypto fusion*, etc.) only involve bijective summation and averaging operations. In simple terms, if a model is represented as a flattened vector M , these algorithms perform coordinate-wise fusion across parties. That is, they add or average the elements at $M[i]$ from all parties — parameters at a given index i can be fused with no dependency on those at any other indices.

By examining the methods of data reconstruction attacks, we observe that a *global* view of model updates is required in the attacks' optimization procedures. The completeness and data-order of model updates are crucial for reconstructing training data. Lack of either will lead to reconstruction failures. On the contrary, as FL aggregation algorithms for DNN training only involve coordinate-wise operations at the parameter granularity, data completeness and ordering are not required.

Therefore, we are able to partition an entire model update into multiple pieces, deploy them to multiple servers, and execute the same fusion algorithms independently across all servers. Furthermore, before aggregation, each partitioned vector can also be shuffled at each training round, as long as all parties permute in the same order. Parties can reverse the permutation and merge the aggregated partitions locally when they receive the aggregated model updates for synchronization.

3.4 AMD SEV

SEV [28] is a confidential computing technology introduced by AMD. It aims to protect security-sensitive workloads in public cloud environments. SEV depends on AMD Secure Memory Encryption (SME) to enable runtime memory encryption. Along with the AMD Virtualization (AMD-V) architecture, SEV can enforce cryptographic isolation between guest VMs and the hypervisor. Therefore, SEV can prevent privileged system administrators, e.g., at the hypervisor level, from accessing the data within the domain of an EVM.

When SEV is enabled, SEV hardware tags all code and data of a VM with an Address Space Identifier (ASID), which is associated with a distinct ephemeral Advanced Encryption Standard (AES) key, called VM Encryption Key (VEK). The keys are managed by the AMD Secure Processor (SP), which is a 32-bit ARM Cortex-A5 micro-controller integrated within the AMD SoC. Runtime memory encryption is performed via on-die memory controllers. Each memory controller has an AES engine that encrypts/decrypts data when it is written to main memory or is read into the SoC. The control over memory page encryption is via page tables. Physical address bit 47, a.k.a., *C-bit*, is used to mark whether the memory page is encrypted.

Similar to other TEEs, SEV also provides a remote attestation mechanism for authenticating hardware platforms and attesting EVMs. The authenticity of the platform is proven with an identity key signed by AMD and the platform owner. Before provisioning any secrets, EVM owners should verify both the authenticity of SEV-enabled hardware and the measurement of Open Virtual Machine Firmware (OVMF), which enables UEFI support for booting EVMs.

4 SYSTEM DESIGN

In this section, we detail the design of TRUDA and demonstrate how it effectively mitigates information leakage channels for FL data reconstruction attacks. We describe three key security mechanisms of TRUDA: (1) enabling trustworthy FL aggregation with a two-phase attestation protocol, (2) separating a central aggregator to multiple decentralized entities, each with only a fragmentary view of the model updates, and (3) shuffling model updates dynamically for each training round. These three mechanisms are composable and can operate with no mutual dependency. Such a multi-faceted design makes TRUDA more resilient when facing unanticipated security breaches. For example, assuming that memory encryption of TEEs is broken due to some new zero-day vulnerabilities, the adversaries will still not be able to reconstruct training data from the model updates (leaked from TEEs) as they are fragmentary and obfuscated with mechanisms (2) and/or (3) enabled.

We give a concrete deployment example of TRUDA in Figure 1 and discuss the workflow step by step. Similar to traditional FL, in TRUDA, each party needs to register with the aggregators to participate in the training. One aggregator initiates the training process by notifying all parties. During training, aggregators engage in a number of training rounds with all parties. At each training round, each party uses its local training data to produce a new model update and upload it to the aggregators. The aggregators merge model updates from all parties and dispatch the aggregated version back to all parties. The global training ends once pre-determined training criteria (like number of epochs or accuracy) are met.

Different from traditional FL, TRUDA’s deployment involves multiple aggregators running within TEEs, rather than a single central aggregator. Aggregators need to communicate with each other for training synchronization. In addition, we also deploy an attestation server as a trusted anchor, which is responsible for attesting the aggregator’s workload and provisioning secrets on behalf of all parties.

4.1 Trustworthy Aggregation

As mentioned earlier, model updates exchanged between parties and aggregators may contain essential information for reverse engineering private training data. We need to eliminate the channels for adversaries to intercept and inspect model updates in transit and also in use. In our design, we enforce cryptographic isolation for FL aggregation via SEV. The aggregators execute within EVMs. Each EVM’s memory is protected with a distinct ephemeral VEK. Therefore, we can protect the confidentiality of model aggregation from unauthorized users, e.g., system administrators, and privileged software running on the hosting servers. AMD provides attestation primitives for verifying the authenticity of individual SEV hardware/firmware. We design a new attestation protocol upon the primitives to bootstrap trust between parties and aggregators in the distributed FL setting. This FL attestation protocol consists of two phases:

Phase 1: Launching Trustworthy Aggregators. First, we need to securely launch SEV EVMs with aggregators running within. To establish the trust of EVMs, attestation must prove that (1) the platform is an authentic AMD SEV-enabled hardware providing the required security properties, and (2) the OVMF image to launch the EVM is not tampered. Once the remote attestation is completed, we can provision a secret, as a unique identifier of a trustworthy aggregator, to the EVM. The secret is injected into EVM’s encrypted physical memory and used for aggregator authentication in Phase 2.

In Figure 1, Step ❶ shows an attestation server that facilitates remote attestation. The EVM owner instructs the AMD SP to export the certificate chain from the Platform Diffie-Hellman Public Key (PDH) down to the AMD Root Key (ARK). This certificate chain can be verified by the AMD root certificates. The digest of OVMF image is also included in the attestation report along with the certificate chain.

The attestation report is sent to the attestation server, which is provisioned with the AMD root certificates. The attestation server verifies the certificate chain to authenticate the hardware platform and check the integrity of OVMF firmware. Thereafter, the attestation server generates a launch blob and a Guest Owner Diffie-Hellman Public Key (GODH) certificate. They are sent back to the SP on the aggregator’s machine for negotiating a Transport Encryption Key (TEK) and a Transport Integrity Key (TIK) through Diffie-Hellman Key Exchange (DHKE) and launching the EVMs.

We can retrieve the OVMF runtime measurement through the SP by pausing the EVM at launch time. We send this measurement (along with the SEV API version and the EVM deployment policy) to the attestation server to prove the integrity of UEFI booting process. Only after verifying the measurement, the attestation server generates a packaged secret, which includes an ECDSA prime251v1 key. The hypervisor injects this secret into the EVM’s physical memory space as a unique identifier of a trusted aggregator and continue the launching process. Our secret injection procedure follows the 1st-generation SEV’s remote attestation protocol. With the upcoming SEV-SNP, AMD SP can also measure and attest the layout of EVM’s initial memory and its contents [48]. Thus, the new SEV-SNP’s attestation mechanism can further reinforce the integrity of the launching process.

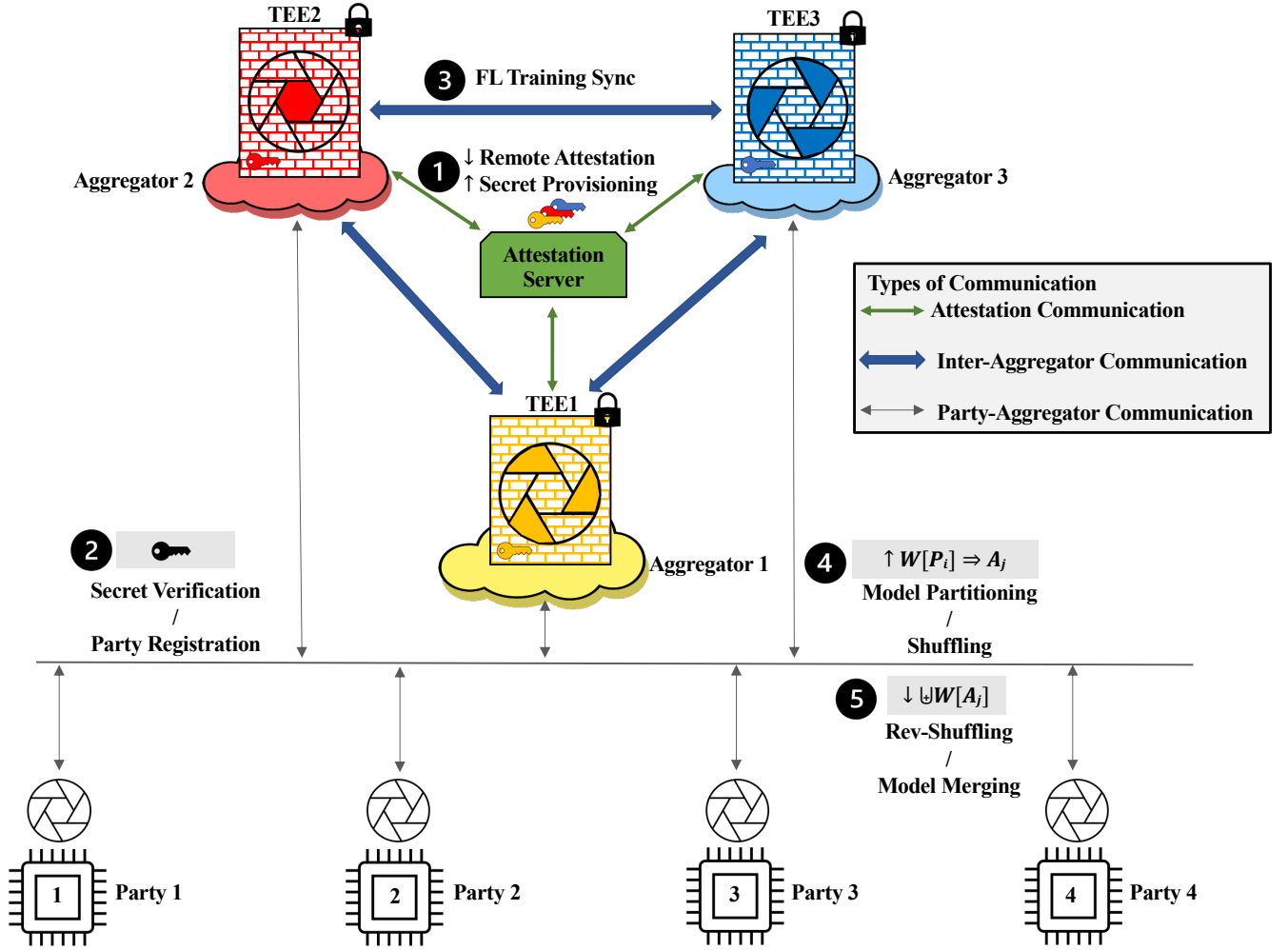


Figure 1: System Architecture of TRUDA

Phase 2: Aggregator Authentication. Parties participating in FL must ensure that they are interacting with trustworthy aggregators with runtime memory encryption protection. To enable aggregator authentication, in Phase 1, the attestation server provisions an ECDSA key as a secret during EVM deployment. This key is used for signing challenge requests and thus serves to identify a legitimate aggregator. In step ② of Figure 1, before participating in FL, a party first attests an aggregator by engaging in a challenge response protocol. The party sends a randomly generated nonce to the aggregator. The aggregator digitally signs the nonce using its corresponding ECDSA key and then returns the signed nonce to the requesting party. The party verifies that the nonce is signed with the corresponding ECDSA key. If the verification is successful, the party then proceeds to register with the aggregator to participate in FL. This process is repeated for all aggregators.

After registration, end-to-end secure channels can be established to protect communications between aggregators and parties for

exchanging model updates. We enable TLS to support mutual authentication between a party and an aggregator. Thus, all model updates are protected both within EVMs and in transit.

4.2 Decentralized Aggregation

Enabling trustworthy aggregation alone may not be sufficient. We cannot expect that TEEs are omnipotent and that there will be no security vulnerabilities discovered in the future. In fact, we have already observed some security breaches with regard to SEV [8, 32, 33, 59, 60]. Therefore, we enhance our design to ensure that even if TEEs are breached, adversaries cannot reconstruct training data from model updates.

Decentralization has been primarily explored (e.g., Bonawitz et al. [6]) in distributed learning as a load balancing technique to address the performance problems with respect to a central server, and to scale to a large number of parties. This has typically involved distributing parties among aggregator replicas (“party-partitioning”), and the replicas co-ordinating among themselves

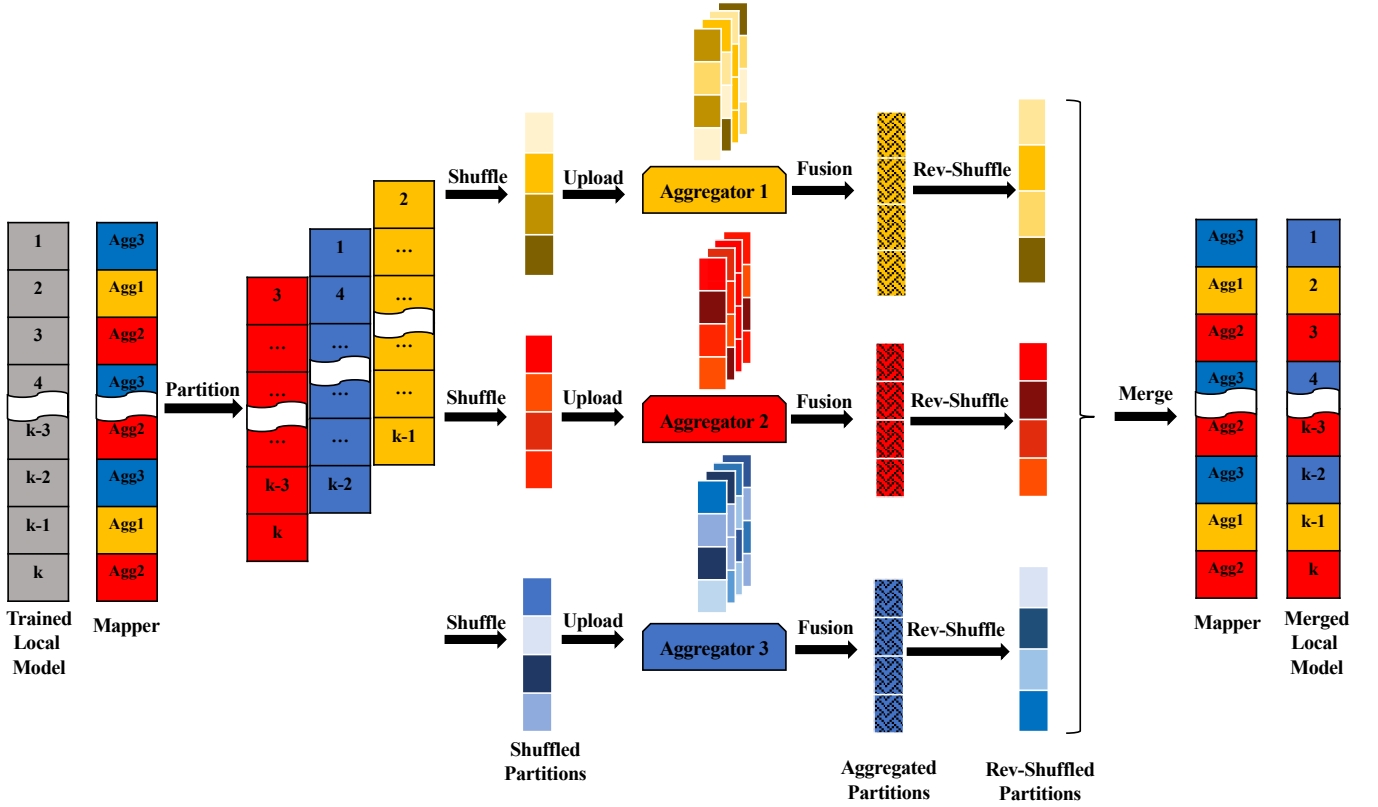


Figure 2: Model Partitioning and Dynamic Permutation

to aggregate intermediate results. In this setting, each model update reaches an aggregator replica in its entirety, making reverse engineering possible. In other research on fully-decentralized/peer-to-peer distributed learning[2, 30, 31, 58], there exists no central aggregator. Each party exchanges model updates with their neighbors and merges the received updates with its local model. But this scheme cannot prevent information leakage either as the entire model updates are still circulated among parties in the network and susceptible to reconstruction attacks.

In TRUDA, we choose a different decentralization strategy with model partitioning enabled. Each aggregator only receives a fraction of each model update and runs within an EVM. For example, in Figure 1, we establish three aggregators. Each party authenticates and registers with all aggregators respectively.

Inter-Aggregator Training Synchronization. We maintain communication channels between aggregators for training synchronization, e.g., step ③ of Figure 1. Any one of the aggregators can start the training and become the *initiator* node by default. All the other aggregators become *follower* nodes and wait for the commands from the *initiator*. At each training round, the *initiator* first notifies all parties to start local training and retrieve the model updates for fusion. Thereafter, it notifies all the *follower* nodes to pull their corresponding model updates, aggregate them together, and distribute the aggregated updates back to the parties.

Randomized Model Partitioning. Due to the bijective nature of FL fusion algorithms, we can split a model update into disjoint partitions based on the number of available aggregators. Before training starts, we randomly generate a model-mapper for each DNN model (to be trained). We allow the parties to choose the proportion of model parameters for each aggregator. This model-mapper is shared by all the parties that participate in the FL training. For example, in Figure 2, the k parameters of a local model are mapped to three aggregators. The colors imply the aggregator attributes for each parameter within the model. The model update is disassembled and rearranged at the parameter-granularity for different aggregators (step ④ in Figure 1). Once parties receive fused model updates from different aggregators, they query the model-mapper again to merge model updates to its original positions within the local model (step ⑤ in Figure 1). A shared model-mapper can be generated either by (i) using a consensus algorithm like Raft, or (ii) constructed at each party using random number generators seeded by the same random value (e.g., from League of Entropy²).

Decentralized aggregation significantly defends against the illegitimate leak of model information at the aggregation point as aggregators no longer store the complete model updates nor the model architectures. As we demonstrate in Section 6, even missing a very small fraction of a model update totally renders the data reconstruction attacks ineffective. Thus, decentralized aggregation

²<https://blog.cloudflare.com/league-of-entropy/>

requires adversaries to compromise all TEE-protected aggregators (which can be isolated in different protected domains) and obtain the model-mapper (protected within party’s training devices) to piece together complete model updates in their original order.

4.3 Shuffled Aggregation

To further obfuscate the information transferred from the parties to the aggregators, we employ a dynamic permutation scheme to shuffle the partitioned model updates at every training round. Each permutation is seeded by the *combination* of a permutation key (e.g., dispatched from a trusted key generation server) agreed among all parties and a dynamically generated training identifier synchronized at the start of each training round. Thus, the permutation changes every training round, but is deterministic across all parties. After parties receive aggregated model updates, they rev-shuffle the results back to their original order as shown in Figure 2.

The dynamic permutation scheme is based on the insight that the data-order of model updates is irrelevant for model-fusion algorithms, while it is crucial for optimization procedures used in data reconstruction attacks. With dynamic permutation enabled, adversaries only obtain obfuscated model updates and the data order dynamically changes at each training round. If the permutation seed is not leaked, it is infeasible for adversaries to reconstruct any training data even if they compromise all TEE-protected aggregators. In addition, this shuffled aggregation mechanism works in the deployments with either a central aggregator (as in traditional FL) or multiple decentralized aggregators (as in TRUDA).

5 IMPLEMENTATION

We developed TRUDA by extending the publicly available IBM Framework for Federated Learning (FFL) [35] to support trustworthy aggregation, decentralized multi-aggregators with model partitioning, and dynamic permutation of model updates. We containerized the aggregator application and employed Kata Container [29] to deploy aggregator containers inside lightweight EVMs. We used an AMD EPYC 7642 (ROME) microprocessor running SEV API Version 0.22 [47]. We extended QEMU with Feldman-Fitzthum’s patch [11]³ to support AMD SEV *LAUNCH_SECRET* and extended Kata-runtime to provide remote attestation via client-side gRPC [14] communication with the attestation server. Finally, We implemented our attestation server as a gRPC service using a modified version of the AMD SEV-Tool [49] to support EVM owners’ tasks, e.g., attesting the AMD SEV-enabled hardware platform, verifying the OVMF launch measurement, and generating the launch blob.

6 SECURITY ANALYSIS

We evaluated the effectiveness of TRUDA against three FL attacks that attempted to reconstruct training data based on model updates: DLG [67], iDLG [63], and IG [12]. We used the implementations from their public git repositories [10, 22, 23] for our experiments. First, we evaluated each attack with only model partitioning enabled, varying the partition factor by 40%, thus lowering the percentage of model updates accessible to the attack. A partition factor of 100% means the attack had access to the entire model update.

Then, we enabled dynamic permutation together with model partitioning and re-evaluated the model, again varying the partition factor by 40%.

The current design of TRUDA does not allow aggregators to maintain a global model, thus they have no knowledge of the model architecture. DLG, iDLG, and IG can neither retrieve the unmodified model updates associated with an input sample nor query the model for the dummy input’s current loss gradients. As such, in a real deployment of TRUDA, these attacks would not succeed as they lack both these two critical components. However, to analyze the effects of the security measures of TRUDA, we relaxed the constraints and allowed adversaries to query the complete, unperturbed model as a blackbox. Therefore, the attacks could compute the dummy inputs’ loss gradients, but the original inputs’ loss gradients were still transformed by TRUDA. In this stronger attack scenario, we demonstrate that TRUDA still remains effective and prevents the attacks from leaking information through reconstructing data from model updates.

6.1 DLG and iDLG Results

We used a randomly initialized *LeNet* model for evaluation as done by prior works [63, 67] and evaluated both attacks using 1000 randomly selected inputs from the *CIFAR-100* dataset. *CIFAR-100* is a dataset with 32×32 color images in 100 classes. We ran each attack for 300 iterations. The effectiveness of TRUDA against DLG and iDLG is reported in Table 1.

We partitioned the results into six ranges based on the Mean Squared Error (MSE) of each image. MSE is the metric adopted in DLG/iDLG for measuring the quality of reconstructed images in *CIFAR-100*. Through visual inspection, an MSE below 1.0×10^{-3} compared to the original images resulted in recognizable reconstructions. We highlight this threshold in red in Table 1. Without TRUDA in place, DLG and iDLG, resulted in generating 66.6% and 83.7% recognizable reconstructions respectively with a partition factor of 100% (i.e., no model partitioning). These results are used as the baseline and highlighted in the two *underlined* columns. However, as soon as model partitioning is enabled, the reconstruction quality drops significantly. Due to model partitioning, both attacks’ estimates of the original gradients are increasingly inaccurate as fewer of the original model’s weights are available. In turn, both attacks cannot correctly minimize the cost function, which we observed during the attack process. With only a 60% partition rate, neither attack is able to generate any recognizable reconstructions. Enabling dynamic permutation in addition to model partitioning adds an additional layer of protection against reconstruction attacks as evidenced by the increased MSE of the reconstructions in Table 1. Even with all of the model weights, neither attack is able to generate an recognizable reconstruction as dynamic permutation of the model weights prevents the attacks from correctly aligning their gradient estimations. In the first and second rows of Figure 3, we present the reconstructions generated by the DLG and iDLG attacks without and with TRUDA enabled for one of the images. In Appendix B, we include another example (Figure 7) with more details of intermediate iterations.

³This patch will be included in the release of QEMU 6.0

Table 1: Comparison of Fidelity Threshold (MSE) for DLG and iDLG with Model Partitioning and Permutation

Fidelity Threshold (MSE)	DLG (w/o perm)			iDLG (w/o perm)			DLG (with perm)			iDLG (with perm)		
	Partition %			Partition %			Partition %			Partition %		
	100	60	20	100	60	20	100	60	20	100	60	20
$[0, 1.0 \times 10^{-3})$	66.6%	0.0%	0.0%	83.7%	0.0%	0.0%	0.0%	0.0%	0.0%	0.0%	0.0%	0.0%
$[1.0 \times 10^{-3}, 1.0 \times 10^{-2})$	0.8%	0.0%	0.0%	1.2%	0.0%	0.0%	0.0%	0.0%	0.0%	0.0%	0.0%	0.0%
$[1.0 \times 10^{-2}, 1.0 \times 10^{-1})$	0.3%	0.0%	0.0%	0.1%	0.0%	0.0%	0.0%	0.0%	0.0%	0.0%	0.0%	0.0%
$[1.0 \times 10^{-1}, 1.0)$	0.2%	0.0%	0.0%	0.2%	0.0%	0.0%	0.0%	0.0%	0.0%	0.0%	0.0%	0.0%
$[1.0, 1.0 \times 10^2)$	8.1%	38.9%	20.5%	6.6%	66.5%	18.3%	0.0%	0.0%	0.2%	0.2%	0.2%	0.7%
$\geq 1.0 \times 10^2$	24.0%	61.1%	79.5%	8.2%	33.5%	81.7%	100.0%	100.0%	99.8%	99.8%	99.8%	99.3%

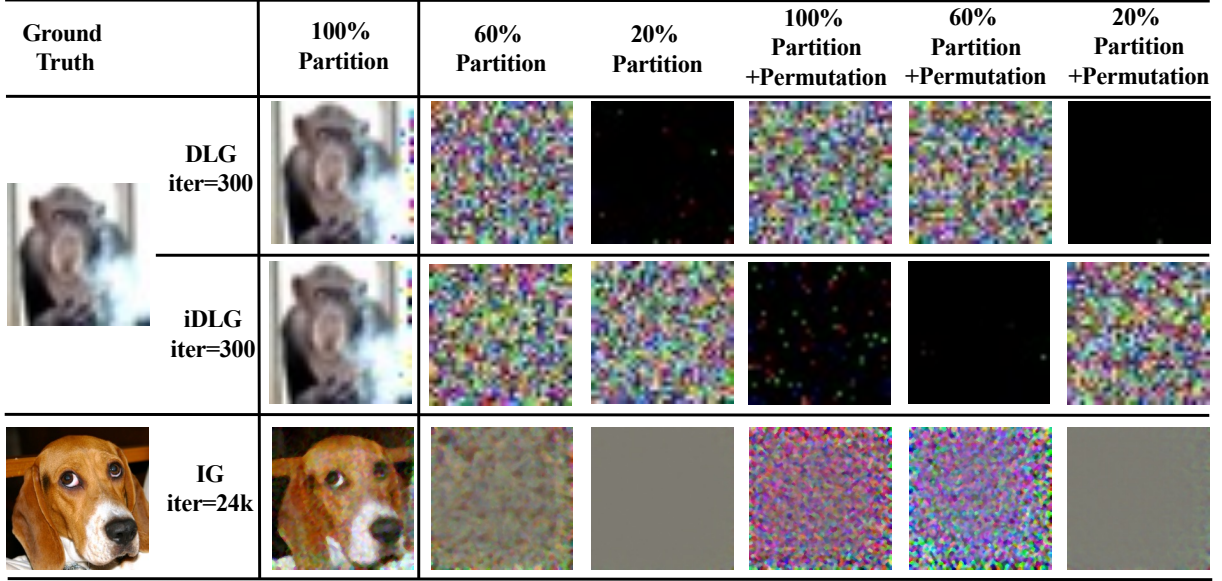


Figure 3: Reconstruction Examples of DLG/iDLG/IG with Model Partitioning and Permutation

Table 2: Comparison of Final Cosine Distance for IG with Model Partitioning and Permutation

Cosine Distance	IG (partition)			IG (partition+perm)		
	Partition %			Partition %		
	100	60	20	100	60	20
$[0, 0.01)$	100%	0%	0%	0%	0%	0%
$[0.01, 0.2)$	0%	0%	0%	0%	0%	0%
$[0.2, 0.4)$	0%	100%	0%	0%	0%	0%
$[0.4, 0.6)$	0%	0%	98%	0%	0%	0%
$[0.6, 0.8)$	0%	0%	2%	0%	0%	0%
$[0.8, 1]$	0%	0%	0%	100%	100%	100%

6.2 IG Results

We used a randomly initialized *ResNet-18* model for evaluation as done by prior work [12] and evaluated IG using 50 randomly selected inputs from the *ImageNet* dataset. *ImageNet* is a dataset with 224×224 color images in 1000 classes. We ran the attack for 24,000 iterations with two random restarts.

The authors of IG remarked that the reconstruction quality and amount of information leaked are highly dependent on the images. MSE is no longer an accurate metric for measuring image similarity for large-sized data samples of *ImageNet*. Instead, we measured the *cosine distance*, which is used as the cost function of IG, to show that TRUDA effectively hinders the optimization procedure. We partitioned the cosine distance (bounded in $[0, 1]$) into six ranges and present the results in Table 2. Without TRUDA in place, the cosine distance of IG’s cost function is always smaller than 0.01 with a partition factor of 100% (i.e., no model partitioning). These results are used as the baseline and highlighted in the column with the underlined values. With TRUDA enabled, IG can no longer correctly minimize the cost function. The cosine distance values in the optimization procedures stuck at the level significantly larger than 0.01. For example, with a 60% partition rate and no permutation, all cosine distance values are in the range of $[0.2, 0.4)$. With permutation enabled, the cosine distance is further increased to the range of $[0.8, 1]$. Visual inspection of the results reveals that IG cannot generate any recognizable reconstructions with TRUDA’s partitioning and permutation in place. In the third row of Figure 3, we present the reconstructions generated by the IG attack without

and with TRUDA enabled for one of the images. In Appendix B, we include five more reconstruction examples for IG in Figure 8.

7 PERFORMANCE EVALUATION

We evaluated the performance of TRUDA with two metrics. First, we measured the loss/accuracy of the models generated at each training round. It demonstrates that the convergence rate of TRUDA is aligned with the base system and TRUDA does not lead to model accuracy degradation. Second, we measured the latency of FL training. The latency of model training refers to the total time to finish a specified number of training rounds. We recorded the time after finishing each training round at the aggregator. The latency results reflect the performance overhead incurred by the security features added in TRUDA.

Our evaluation covers a spectrum of *cross-silo* FL training applications from three aspects: (1) adaptability to different FL aggregation algorithms, (2) performance comparisons with different numbers of participating parties, and (3) support for larger DNN models with non-IID training data distribution.

In our evaluation environment, each party ran within a VM in a datacenter. We assigned each VM with 16 cores of Intel Xeon E5-2690 CPU, one Nvidia Tesla P100 GPU, 120 GB DRAM; the OS is Redhat Enterprise Linux 7.0-64. We set up three aggregators to run within the SEV EVMs. The aggregators ran on a machine with AMD EPYC 7642 CPU; the host OS is Ubuntu 20.04 LTS. The baseline for comparison is IBM FFL with one central aggregator. The party’s configurations, model architectures, and hyper-parameter settings are the same as for TRUDA and FFL.

7.1 Training with Different Fusion Algorithms

As indicated in the TRUDA’s design, we support aggregation algorithms with coordinate-wise arithmetic operations. We evaluated TRUDA respectively with three aggregation algorithms, i.e., *Iterative Averaging*, *Coordinate Median*[61], and *Paillier*[34, 53], with the *MNIST* dataset. *Iterative Averaging* is the base algorithm supporting *FedAvg* and *FedSGD*. It sends queries to all registered parties at each training round to collect information, e.g., model updates or gradients, averages the updates, and broadcasts the fused results to all parties. *Coordinate Median* is a fusion algorithm that selects a coordinate-wise median from collected responses in order to tolerate Byzantine failures of adversarial parties. The *Paillier crypto fusion* algorithm supports aggregation with Additively Homomorphic Encryption[44]. We trained deep learning models on the *MNIST* dataset with ten training rounds for *Iterative Averaging*, *Coordinate Median* and three rounds for *Paillier*. Each round has three local epochs.

MNIST contains 60,000 examples in the training set. We randomly partitioned the training set into four equal sets for four parties. Each party has 15,000 examples for local training. The trained model is a convolutional neural network (ConvNet) with eight layers. The detailed model architecture can be found in Table 3 of Appendix A.

Accuracy/Loss and Convergence Rate. We present the model loss and accuracy at each training round in Figures 4a, 4b, and 4c. The horizontal axes are the number of training rounds. The left vertical axes show the loss and the right vertical axes present the

model accuracy. It is clear that the loss/accuracy results of TRUDA and FFL have the same patterns for all three fusion algorithms. TRUDA and FFL converge at the same rate on *MNIST* after one training round. The final models achieve the same accuracy level (above 98%) for both TRUDA and FFL.

Training Latency. We present the training latency data of TRUDA and FFL in Figures 4d, 4e, and 4f. The vertical axes are the accumulated time spent to finish that training round. We observed that for *Iterative Averaging*, TRUDA used 75.83 seconds to finish the 10-round training and FFL used 54.32 seconds. Compared to the baseline FFL system, the added security features in TRUDA incurred additional 0.40 \times latency for training the *MNIST* model. Similarly for *Coordinate Median*, TRUDA incurred additional 0.45 \times in latency.

Due to heavyweight additively homomorphic encryption operations, *Paillier crypto fusion* is two orders slower for training the same *MNIST* model than *Iterative Averaging* and *Coordinate Median*. However, TRUDA finished training with 0.04 \times improvement in latency compared to FFL. The reason is that the dominant performance factors of *Paillier* fusion are the encryption/decryption operations. However, as the models are partitioned in TRUDA for multiple decentralized aggregators, the *Paillier* encryption/decryption and aggregation are accelerated — computed in parallel by operating on smaller model partitions both on the aggregators and on the parties.

7.2 Training with Different Numbers of Parties

Here, we aim to understand the performance effects of involving more parties. We trained a ConvNet with 23 layers on *CIFAR-10* with four and eight parties. The detailed model architecture can be found in Table 4 in Appendix A. *CIFAR-10* is a dataset with 32×32 color images in 10 classes. We randomly partition the training set into equal sets for the parties. Each party has 10,000 examples for FL training. We trained this model with 30 training rounds, with each round consisting of one local epoch.

Accuracy/Loss and Convergence Rate. We present the model accuracy and loss at each training round in Figure 5a. The patterns for the loss and accuracy are similar for TRUDA and FFL with both four parties and eight parties. It indicates that the models converge at a similar rate with different number of parties. The accuracy results of the final model trained with FFL are 76.99% (four parties) and 76.43% (eight parties). The final model accuracy results with TRUDA are 79.93% (four parties) and 81.41% (eight parties).

Training Latency. We present the training latency data of TRUDA and FFL in Figure 5b. In the four parties scenario, it took TRUDA 182.91 seconds to finish 30 rounds of training and FFL 157.41 seconds. Our added features incurred additional 0.16 \times in latency for training the *CIFAR-10* model. In the eight parties scenario, it took TRUDA 498.68 seconds to finish 30 rounds of training and FFL 477.34 seconds. The latency only increased by 0.04 \times . We also find that adding more parties increases the latency for both FFL and TRUDA at the same pace. The security features of TRUDA does not lead to additional latency with regard to more parties.

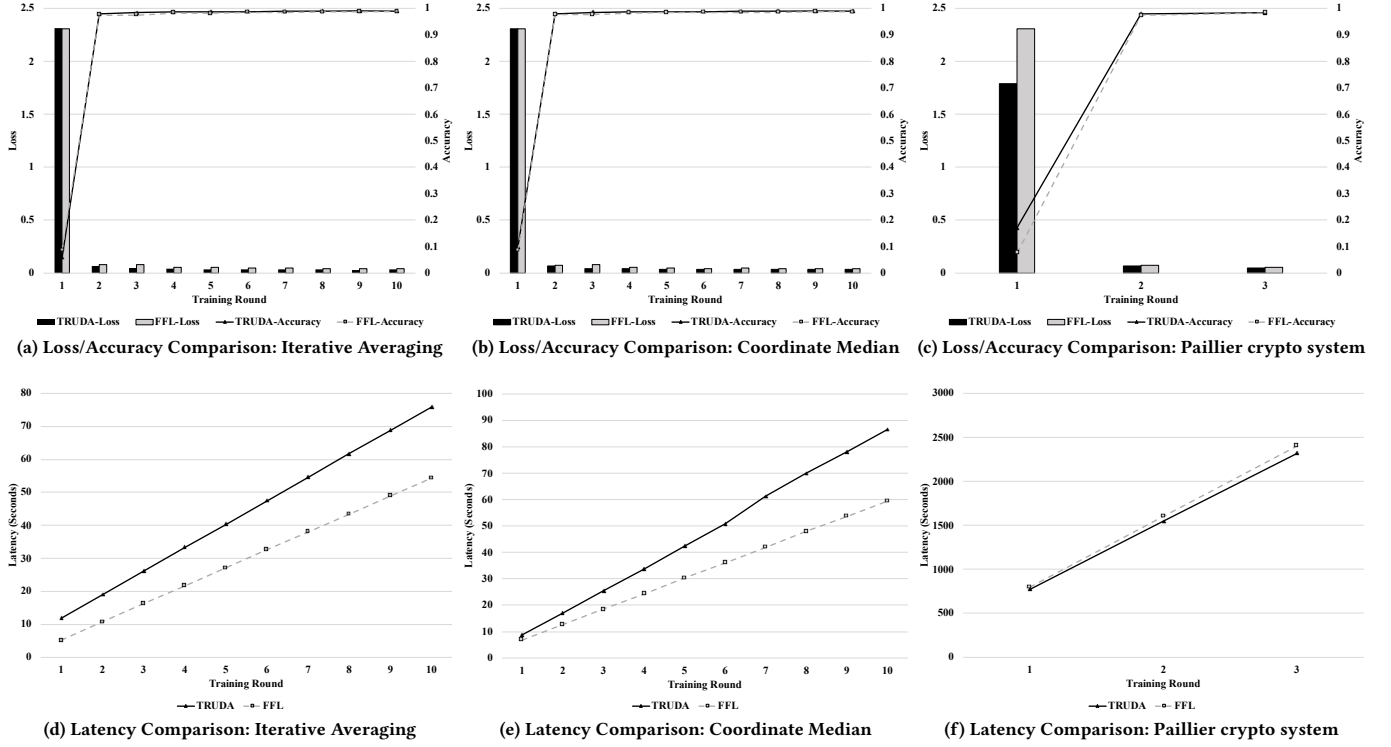


Figure 4: MNIST Loss/Accuracy/Latency Comparison Between TRUDA and FFL (IID with Four Parties)

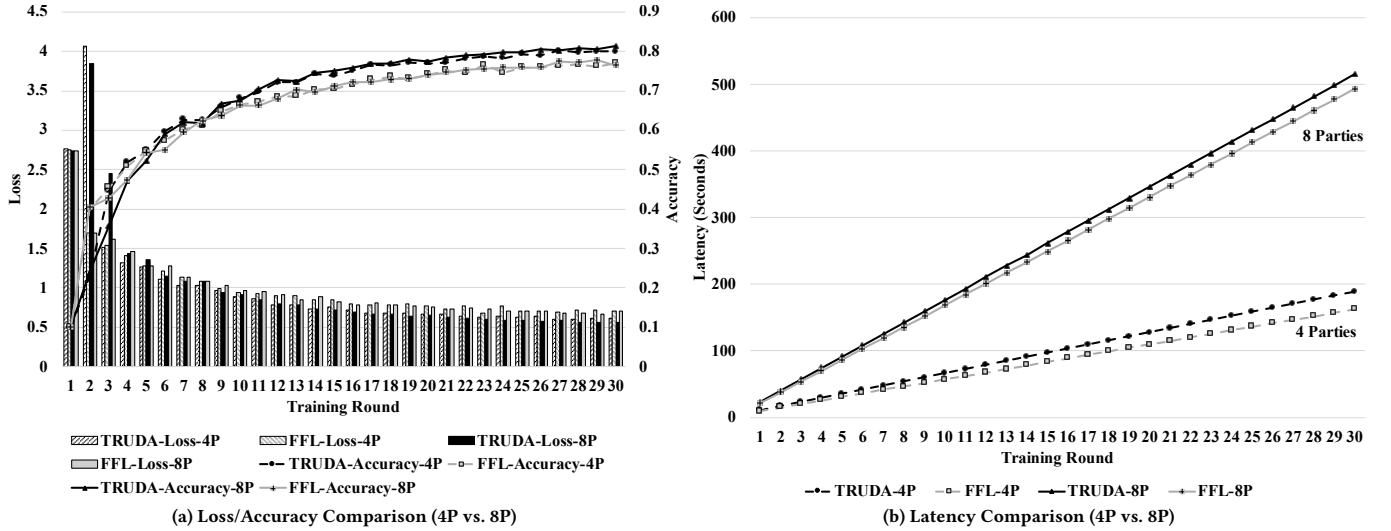


Figure 5: CIFAR10 Loss/Accuracy/Latency Comparison Between TRUDA and FFL (IID with Four/Eight Parties)

7.3 Training with Non-IID Training Data

We also measured the performance of training a larger, more complex deep learning model with non-IID training data distribution. We used a pre-trained *VGG-16* model on the *ImageNet* to train a document classifier on the *RVL-CDIP*[18] dataset with 16 classes.

For transfer learning with *RVL-CDIP* classification, we replaced the last three fully-connected layers of *VGG-16* due to differences in number of prediction classes. The detailed model architecture can be found in Table 5 in Appendix A. The *RVL-CDIP* dataset has 320,000 training images and 40,000 test images. We partitioned the

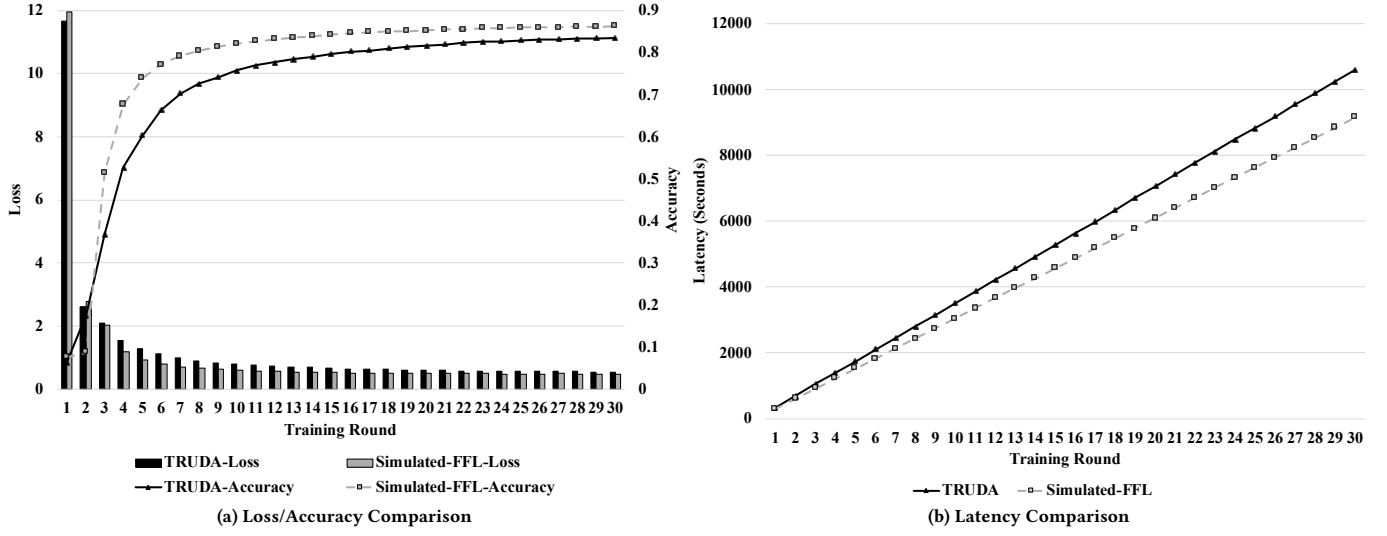


Figure 6: RVL-CDIP Loss/Accuracy/Latency Comparison Between TRUDA and FFL (non-IID with Eight Parties)

training data based on the non-IID 90-10 skew data split for eight parties. Each party has approximately 40,000 training examples with skew distribution among different classes, i.e., the two dominant classes contain 90% of training data, while the remaining 14 classes have 10%. We trained deep learning models with 30 training rounds. Each round has one epoch. As *RVL-CDIP* dataset it not officially supported in FFL, we simulated the FFL implementation for performance comparison.

Accuracy/Loss and Convergence Rate. We present the model accuracy and loss at each training round in Figure 6a. Similarly, the models converge at a similar rate with TRUDA and FFL. The accuracy results of the final model trained with TRUDA is 83.50% and 86.19% with simulated FFL.

Training Latency. We present the training latency data of TRUDA and simulated FFL in Figure 6b. It took TRUDA 2.85 hours and FFL 2.46 hours to finish 30 rounds of training. Our added security features in TRUDA incurred additional 0.16 \times in latency for training the *RVL-CDIP* model.

8 RELATED WORK

In this section, we give an overview of the security defenses against the FL privacy leakage attacks and analyze their pros and cons from the perspectives of security and utility trade-off. In addition, we compare TRUDA with them to demonstrate the contributions of our work.

8.1 Trusted Execution Environments

TEEs allow users to out-source their computation to third-party cloud servers with trust on the CPU package. They are particularly attractive for collaborative ML computation, which may involve a large amount of privacy-sensitive training data, multiple distrusting parties, and stricter data protection regulations. TEEs can act as trustworthy intermediaries for isolating and orchestrating ML

processes and replace the expensive cryptographic primitives. For example, Software Guard Extensions (SGX) has been leveraged to support secure model inference [15, 52], privacy-preserving multi-party machine learning [16, 20, 21, 40, 43], and analytics on sensitive data [4, 9, 46, 64].

However, TEEs are not panacea to address all trust problems. Existing TEE technologies have different performance and capacity constraints. For example, SGX has a limit (128 MB) on the enclave’s physical memory size. 1st-generation SEV does not provide integrity protection. External ML accelerators cannot be exploited for trusted execution with runtime memory encryption. In addition, TEEs may still be susceptible to emerging security vulnerabilities [8, 32, 33, 42, 54–57, 59, 60]. One small defect may break the foundation of the entire trustworthy system. Thus, to assess a TEE-integrated system, we need to distinguish security properties of different TEEs and extend the threat model in case of TEE failure.

Sharing a similar goal with all the research works mentioned above, we leverage TEEs to support trustworthy aggregation as the first-line defense against privacy leakages. The unique contributions of our work are to decentralize the aggregation to multiple trusted execution entities and employ dynamic permutation to further obfuscate the model updates. Thus, we are still resilient to data reconstruction attacks even if model updates are leaked from breached TEEs.

8.2 Cryptographic Schemes

Homomorphic Encryption allows arithmetic operations on ciphertexts without decryption. Aono et al. [1] used additively HE to protect the privacy of gradients to prevent information leakage. Hardy et al. [17] encrypted vertically partitioned data with an additively HE and learned a linear classifier in the FL setting. Secure Multi-Party Computation allows different parties to compute a joint function without revealing their inputs to each other and has

been widely researched in collaborative analytics and multi-party learning [7, 7, 41, 45, 53, 65, 66].

Compared to TEE-based approaches like TRUDA, using cryptographic schemes for privacy protection promise same-level privacy/accuracy and can exclude CPU vendors from the trust domain. But the trade-offs are the extra communication and computational overhead. The performance constraints for now may still hinder their applications for large-scale FL training scenarios.

8.3 Differential Privacy

In the ML setting, DP can be used to apply perturbations for mitigating information leakage. Compared to cryptographic schemes, DP is more computationally efficient at the cost of a certain utility loss due to the added noise. Centralized Differential Privacy (CDP) data analysis is typically conducted under the assumption of a trusted central server. CDP [13, 38] can achieve an acceptable balance between privacy and accuracy, but it does not fit a threat model where the aggregation server might be honest-but-curious, malicious, or compromised. In an effort to remove the trusted central server assumption in the threat model, Local Differential Privacy (LDP) [3, 50] lets each client conduct differentially private transformations of their private data before sharing them with the aggregator. However, achieving LDP comes at the cost of utility loss as every participant must add enough noise to ensure DP in isolation.

Due to conflicting threat models, the design of decentralized and shuffled aggregation in TRUDA is incompatible with CDP, which requires a central aggregator in FL training. However, we can still enable trustworthy aggregation to strengthen CDP with a TEE-protected aggregator. TRUDA can be seamlessly integrated with LDP as the LDP's perturbations only apply to model updates on the party machines.

9 CONCLUSION

In light of the recent training data reconstruction attacks targeting FL aggregation, we rethink the trust model and system architecture of FL frameworks and identify the root causes of their susceptibility to such attacks. To address the problem, we exploit the unique computational properties of aggregation algorithms and propose protocol/architectural enhancements to minimize the leakage surface and break the information concentration. We have developed TRUDA, a new cross-silo FL system encompassing three security-reinforced mechanisms, i.e., trustworthy, decentralized, and shuffled aggregation. Therefore, each aggregator only has a fragmentary and obfuscated view of the model updates. We demonstrate that TRUDA can effectively mitigate all training data reconstruction attacks with no utility loss and low performance overheads.

REFERENCES

- [1] Yoshinori Aono, Takuya Hayashi, Lihua Wang, Shihō Moriai, et al. 2017. Privacy-preserving deep learning via additively homomorphic encryption. *IEEE Transactions on Information Forensics and Security* 13, 5 (2017), 1333–1345.
- [2] Aurélien Bellet, Rachid Guerraoui, Mahsa Taziki, and Marc Tommasi. 2018. Personalized and private peer-to-peer machine learning. In *International Conference on Artificial Intelligence and Statistics*. PMLR, 473–481.
- [3] Abhishek Bhowmick, John Duchi, Julien Freudiger, Gaurav Kapoor, and Ryan Rogers. 2018. Protection against reconstruction and its applications in private federated learning. *arXiv preprint arXiv:1812.00984* (2018).
- [4] Andrea Bittau, Úlfar Erlingsson, Petros Maniatis, Ilya Mironov, Ananth Raghunathan, David Lie, Mitch Rudominer, Ushasree Kode, Julien Tinnes, and Bernhard Seefeld. 2017. Prochlo: Strong privacy for analytics in the crowd. In *Proceedings of the 26th Symposium on Operating Systems Principles*. ACM, 441–459.
- [5] Peva Blanchard, El Mahdi El Mhamdi, Rachid Guerraoui, and Julien Stainer. 2017. Machine learning with adversaries: Byzantine tolerant gradient descent. In *Proceedings of the 31st International Conference on Neural Information Processing Systems*. 118–128.
- [6] Keith Bonawitz, Hubert Eichner, Wolfgang Grieskamp, Dmitriy Huba, Alex Ingerman, Vladimir Ivanov, Chloe Kiddon, Jakub Konečný, Stefano Mazzocchi, H Brendan McMahan, et al. 2019. Towards federated learning at scale: System design. *arXiv preprint arXiv:1902.01046* (2019).
- [7] Keith Bonawitz, Vladimir Ivanov, Ben Kreuter, Antonio Marcedone, H Brendan McMahan, Sarvar Patel, Daniel Ramage, Aaron Segal, and Karn Seth. 2017. Practical secure aggregation for privacy-preserving machine learning. In *Proceedings of the 2017 ACM SIGSAC Conference on Computer and Communications Security*. ACM, 1175–1191.
- [8] Robert Buhren, Christian Werling, and Jean-Pierre Seifert. 2019. Insecure Until Proven Updated: Analyzing AMD SEV's Remote Attestation. In *Proceedings of the 2019 ACM SIGSAC Conference on Computer and Communications Security*. ACM, 1087–1099.
- [9] Ankur Dave, Chester Leung, Raluca Ada Popa, Joseph E Gonzalez, and Ion Stoica. 2020. Oblivious cooperative analytics using hardware enclaves. In *Proceedings of the Fifteenth European Conference on Computer Systems*. ACM, 1–17.
- [10] DLG git repository 2020. Deep Leakage From Gradients. <https://github.com/mit-han-lab/dlg>.
- [11] Tobin Feldman-Fitzthum. 2020. sev: add sev-inject-launch-secret. <https://git.qemu.org/?p=qemu.git;a=commit;h=c7f7e6970d3b74c1454cafea4918187e06c473eb>.
- [12] Jonas Geiping, Hartmut Bauermeister, Hannah Dröge, and Michael Moeller. 2020. Inverting Gradients—How easy is it to break privacy in federated learning? *arXiv preprint arXiv:2003.14053* (2020).
- [13] Robin C Geyer, Tassilo Klein, and Moin Nabi. 2017. Differentially private federated learning: A client level perspective. *arXiv preprint arXiv:1712.07557* (2017).
- [14] gRPC 2021. A high performance, open source universal RPC framework. <https://grpc.io/>.
- [15] Zhongshu Gu, Heqing Huang, Jialong Zhang, Dong Su, Hani Jamjoom, Ankita Lamba, Dimitrios Pendarakis, and Ian Molloy. 2018. Confidential Inference via Ternary Model Partitioning. *arXiv preprint arXiv:1807.00969* (2018).
- [16] Zhongshu Gu, Hani Jamjoom, Dong Su, Heqing Huang, Jialong Zhang, Tengfei Ma, Dimitrios Pendarakis, and Ian Molloy. 2019. Reaching data confidentiality and model accountability on the caltrain. In *49th Annual IEEE/IFIP International Conference on Dependable Systems and Networks*. IEEE, 336–348.
- [17] Stephen Hardy, Wilko Henecka, Hamish Ivey-Law, Richard Nock, Giorgio Patrini, Guillaume Smith, and Brian Thorne. 2017. Private federated learning on vertically partitioned data via entity resolution and additively homomorphic encryption. *arXiv preprint arXiv:1711.10677* (2017).
- [18] Adam W Harley, Alex Ufkes, and Konstantinos G Derpanis. 2015. Evaluation of Deep Convolutional Nets for Document Image Classification and Retrieval. In *International Conference on Document Analysis and Recognition*. IEEE, 991–995.
- [19] Guernsey D. H. Hunt, Ramachandra Pai, Michael Le, Hani Jamjoom, Sukadev Bhattiprolu, Rick Boivie, Laurent Dufour, Brad Frey, Mohit Kapur, Kenneth A. Goldman, Ryan Grimm, Janani Janakiraman, John M. Ludden, Paul Mackerras, Cathy May, Elaine R. Palmer, Bharata Bhasker Rao, Lance Roy, William A. Starke, Jeff Stuecheli, Ray Valdez, and Wendel Voigt. 2021. Confidential Computing for OpenPOWER. In *Proceedings of the Sixteenth European Conference on Computer Systems*. ACM, 294–310.
- [20] Tyler Hunt, Congzheng Song, Reza Shokri, Vitaly Shmatikov, and Emmett Witchel. 2018. Chiron: Privacy-preserving Machine Learning as a Service. *arXiv preprint arXiv:1803.05961* (2018).
- [21] Nick Hynes, Raymond Cheng, and Dawn Song. 2018. Efficient Deep Learning on Multi-Source Private Data. *arXiv preprint arXiv:1807.06689* (2018).
- [22] iDLG git repository 2020. Improved Deep Leakage from Gradients. <https://github.com/PatrickZH/Improved-Deep-Leakage-from-Gradients>.
- [23] IG git repository 2020. Inverting Gradients - How easy is it to break Privacy in Federated Learning? <https://github.com/JonasGeiping/invertinggradients>.
- [24] Intel. 2020. Intel Trust Domain Extensions. <https://software.intel.com/content/dam/develop/external/us/en/documents/tdx-whitepaper-final9-17.pdf>. *White paper* (2020).
- [25] K. R. Jayaram, Archit Verma, Ashish Verma, Gegi Thomas, and Colin Sutter-Shepard. 2020. MYSTIKO: Cloud-Mediated, Private, Federated Gradient Descent. In *2020 IEEE 13th International Conference on Cloud Computing (CLOUD)*. IEEE, 201–210.
- [26] Peter Kairouz, H Brendan McMahan, Brendan Avent, Aurélien Bellet, Mehdi Bennis, Arjun Nitin Bhagoji, Keith Bonawitz, Zachary Charles, Graham Cormode, Rachel Cummings, et al. 2019. Advances and open problems in federated learning. *arXiv preprint arXiv:1912.04977* (2019).
- [27] David Kaplan. 2017. Protecting vm register state with sev-es. *White paper* (2017).

- [28] David Kaplan, Jeremy Powell, and Tom Woller. 2016. AMD memory encryption. *White paper* (2016).
- [29] Kata Containers 2021. The speed of containers, the security of VMs. <https://katacontainers.io>.
- [30] Anastasia Koloskova, Sebastian Stich, and Martin Jaggi. 2019. Decentralized stochastic optimization and gossip algorithms with compressed communication. In *International Conference on Machine Learning*. PMLR, 3478–3487.
- [31] Anusha Lalitha, Osman Cihan Kilinc, Tara Javidi, and Farinaz Koushanfar. 2019. Peer-to-peer federated learning on graphs. *arXiv preprint arXiv:1901.11173* (2019).
- [32] Mengyuan Li, Yinqian Zhang, and Zhiqiang Lin. 2020. CROSSLINE: Breaking "Security-by-Crash" based Memory Isolation in AMD SEV. *arXiv preprint arXiv:2008.00146* (2020).
- [33] Mengyuan Li, Yinqian Zhang, Zhiqiang Lin, and Yan Solihin. 2019. Exploiting unprotected I/O operations in AMD's Secure Encrypted Virtualization. In *28th USENIX Security Symposium*. USENIX, 1257–1272.
- [34] Changchang Liu, Supriyo Chakraborty, and Dinesh Verma. 2019. Secure model fusion for distributed learning using partial homomorphic encryption. In *Policy-Based Autonomic Data Governance*. Springer, 154–179.
- [35] Heiko Ludwig, Nathalie Baracaldo, Gegi Thomas, Yi Zhou, Ali Anwar, Shashank Rajamoni, Yuya Ong, Jayaram Radhakrishnan, Ashish Verma, Mathieu Sinn, Mark Purcell, Ambrish Rawat, Tran Minh, Naoise Holohan, Supriyo Chakraborty, Shalisha Whitherspoon, Dean Steuer, Laura Wynter, Hifaz Hassan, Sean Laguna, Mikhail Yurochkin, Mayank Agarwal, Ebube Chuba, and Annie Abay. 2020. IBM Federated Learning: an Enterprise Framework White Paper V0.1. *arXiv preprint arXiv:2007.10987* (2020).
- [36] Frank McKeen, Ilya Alexandrovich, Alex Berenzon, Carlos V Rozas, Hisham Shafi, Vedvyas Shanbhogue, and Uday R Savagaonkar. 2013. Innovative instructions and software model for isolated execution. *The Second Workshop on Hardware and Architectural Support for Security and Privacy* 10, 1 (2013).
- [37] Brendan McMahan, Eider Moore, Daniel Ramage, Seth Hampson, and Blaise Aguerre y Arcas. 2017. Communication-efficient learning of deep networks from decentralized data. In *Artificial Intelligence and Statistics*. PMLR, 1273–1282.
- [38] H Brendan McMahan, Daniel Ramage, Kunal Talwar, and Li Zhang. 2017. Learning differentially private recurrent language models. *arXiv preprint arXiv:1710.06963* (2017).
- [39] Luca Melis, Congzheng Song, Emiliano De Cristofaro, and Vitaly Shmatikov. 2019. Exploiting unintended feature leakage in collaborative learning. In *2019 IEEE Symposium on Security and Privacy*. IEEE, 691–706.
- [40] Fan Mo, Hamed Haddadi, Kleomenis Katevas, Eduard Marin, Diego Perino, and Nicolas Kourtellis. 2021. PPFL: Privacy-preserving Federated Learning with Trusted Execution Environments. *arXiv preprint arXiv:2104.14380* (2021).
- [41] Payman Mohassel and Yupeng Zhang. 2017. Secureml: A system for scalable privacy-preserving machine learning. In *2017 IEEE Symposium on Security and Privacy*. IEEE, 19–38.
- [42] Kit Murdock, David Oswald, Flavio D Garcia, Jo Van Bulck, Daniel Gruss, and Frank Piessens. 2020. Plundervolt: Software-based fault injection attacks against Intel SGX. In *2020 IEEE Symposium on Security and Privacy*. IEEE, 1466–1482.
- [43] Olga Ohrimenko, Felix Schuster, Cédric Fournet, Aastha Mehta, Sebastian Nowozin, Kapil Vaswani, and Manuel Costa. 2016. Oblivious Multi-Party Machine Learning on Trusted Processors. In *25th USENIX Security Symposium*. USENIX, 619–636.
- [44] Pascal Paillier. 1999. Public-key cryptosystems based on composite degree residuosity classes. In *International conference on the theory and applications of cryptographic techniques*. Springer, 223–238.
- [45] Rishabh Poddar, Sukrit Kalra, Avishay Yanai, Ryan Deng, Raluca Ada Popa, and Joseph M Hellerstein. 2021. Senate: A Maliciously-Secure {MPC} Platform for Collaborative Analytics. In *30th USENIX Security Symposium*. USENIX.
- [46] Felix Schuster, Manuel Costa, Cédric Fournet, Christos Gkantsidis, Marcus Peinado, Gloria Mainar-Ruiz, and Mark Russinovich. 2015. VC3: Trustworthy data analytics in the cloud using SGX. In *2015 IEEE Symposium on Security and Privacy*. IEEE, 38–54.
- [47] SEV API 2019. Secure Encrypted Virtualization API Version 0.22. <https://developer.amd.com/wp-content/resources/55766.PDF>.
- [48] AMD SEV-SNP. 2020. Strengthening VM isolation with integrity protection and more. *White Paper* (2020).
- [49] SEV-Tool 2019. SEV-Tool. <https://github.com/AMDESE/sev-tool>.
- [50] Reza Shokri and Vitaly Shmatikov. 2015. Privacy-preserving deep learning. In *Proceedings of the 22nd ACM SIGSAC conference on computer and communications security*. ACM, 1310–1321.
- [51] Christian Szegedy, Wojciech Zaremba, Ilya Sutskever, Joan Bruna, Dumitru Erhan, Ian Goodfellow, and Rob Fergus. 2013. Intriguing properties of neural networks. *arXiv preprint arXiv:1312.6199* (2013).
- [52] Florian Tramèr and Dan Boneh. 2018. Slalom: Fast, Verifiable and Private Execution of Neural Networks in Trusted Hardware. *arXiv preprint arXiv:1806.03287* (2018).
- [53] Stacey Truex, Nathalie Baracaldo, Ali Anwar, Thomas Steinke, Heiko Ludwig, Rui Zhang, and Yi Zhou. 2019. A hybrid approach to privacy-preserving federated learning. In *Proceedings of the 12th ACM Workshop on Artificial Intelligence and Security*. ACM, 1–11.
- [54] Jo Van Bulck, Marina Minkin, Ofir Weisse, Daniel Genkin, Baris Kasikci, Frank Piessens, Mark Silberstein, Thomas F Wenisch, Yuval Yarom, and Raoul Strackx. 2018. Foreshadow: Extracting the keys to the intel {SGX} kingdom with transient out-of-order execution. In *27th USENIX Security Symposium*. USENIX, 991–1008.
- [55] Jo Van Bulck, Daniel Moghimi, Michael Schwarz, Moritz Lipp, Marina Minkin, Daniel Genkin, Yarom Yuval, Berk Sunar, Daniel Gruss, and Frank Piessens. 2020. LVI: Hijacking Transient Execution through Microarchitectural Load Value Injection. In *2020 IEEE Symposium on Security and Privacy*. IEEE, 54–72.
- [56] Stephan van Schaik, Andrew Kwong, Daniel Genkin, and Yuval Yarom. 2020. SGAXe: How SGX fails in practice.
- [57] Stephan van Schaik, Marina Minkin, Andrew Kwong, Daniel Genkin, and Yuval Yarom. 2020. CacheOut: Leaking data on Intel CPUs via cache evictions. *arXiv preprint arXiv:2006.13353* (2020).
- [58] Paul Vanhaesebrouck, Aurélien Bellet, and Marc Tommasi. 2017. Decentralized collaborative learning of personalized models over networks. In *Artificial Intelligence and Statistics*. PMLR, 509–517.
- [59] Jan Werner, Joshua Mason, Manos Antonakakis, Michalis Polychronakis, and Fabian Monrose. 2019. The SEVEREST Of Them All: Inference Attacks Against Secure Virtual Enclaves. In *Proceedings of the 2019 ACM Asia Conference on Computer and Communications Security*. ACM, 73–85.
- [60] Luca Wilke, Jan Wichelmann, Mathias Morbitzer, and Thomas Eisenbarth. 2020. SEVurity: No Security Without Integrity—Breaking Integrity-Free Memory Encryption with Minimal Assumptions. *arXiv preprint arXiv:2004.11071* (2020).
- [61] Dong Yin, Yudong Chen, Ramchandran Kannan, and Peter Bartlett. 2018. Byzantine-robust distributed learning: Towards optimal statistical rates. In *International Conference on Machine Learning*. PMLR, 5650–5659.
- [62] Hongxu Yin, Arun Mallya, Arash Vahdat, Jose M Alvarez, Jan Kautz, and Pavlo Molchanov. 2021. See through Gradients: Image Batch Recovery via GradInversion. *arXiv preprint arXiv:2104.07586* (2021).
- [63] Bo Zhao, Konda Reddy Mopuri, and Hakan Bilen. 2020. iDLG: Improved Deep Leakage from Gradients. *arXiv preprint arXiv:2001.02610* (2020).
- [64] Wenting Zheng, Ankur Dave, Jethro G Beekman, Raluca Ada Popa, Joseph E Gonzalez, and Ion Stoica. 2017. Opaque: An oblivious and encrypted distributed analytics platform. In *14th USENIX Symposium on Networked Systems Design and Implementation*. USENIX, 283–298.
- [65] Wenting Zheng, Ryan Deng, Weikeng Chen, Raluca Ada Popa, Aurojit Panda, and Ion Stoica. 2021. Cerebro: A Platform for Multi-Party Cryptographic Collaborative Learning. In *30th USENIX Security Symposium*. USENIX.
- [66] Wenting Zheng, Raluca Ada Popa, Joseph E Gonzalez, and Ion Stoica. 2019. Helen: Maliciously secure cooperative learning for linear models. In *2019 IEEE Symposium on Security and Privacy*. IEEE, 724–738.
- [67] Ligeng Zhu, Zhijian Liu, and Song Han. 2019. Deep leakage from gradients. In *Advances in Neural Information Processing Systems*. 14774–14784.

A TABLES FOR DNN ARCHITECTURES IN FL TRAINING

Here we present the detailed model architectures and hyper-parameters for the three DNNs we trained in Section 7. The *Layer* column shows the layer types, including convolutional layer (conv), dense layer (dense), flatten layer (flat), max pooling layer (maxpool), batch normalization layer (batchnorm), and dropout layer (dropout). The *Filter* column shows the number of filters in each convolutional layer. The *Size* column is in the format of $width \times height$ to represent filter parameters. The *Activation* column shows the type of activation function used.

Table 3: DNN Architecture for MNIST

Layer	Filter	Size	Activation
1 conv	32	3x3	relu
2 conv	64	3x3	relu
3 maxpool		2x2	
4 dropout	p = 0.25		
5 flatten			
6 dense	128		relu
7 dropout	p = 0.50		
8 dense	10		softmax

Table 4: DNN Architecture for CIFAR-10

Layer	Filter	Size	Activation
1 conv	32	3x3	relu
2 batchnorm			
3 conv	32	3x3	relu
4 batchnorm			
5 maxpool		2x2	
6 dropout	p = 0.20		
7 conv	64	3x3	relu
8 batchnorm			
9 conv	64	3x3	relu
10 batchnorm			
11 maxpool		2x2	
12 dropout	p = 0.30		
13 conv	128	3x3	relu
14 batchnorm			
15 conv	128	3x3	relu
16 batchnorm			
17 maxpool		2x2	
18 dropout	p = 0.40		
19 flatten			
20 dense	128		relu
21 batchnorm			
22 dropout	p = 0.50		
23 dense	10		softmax

Table 5: DNN Architecture for RVL-CDIP

Layer	Filter	Size	Activation
1 conv	64	3x3	relu
2 conv	64	3x3	relu
3 maxpool		2x2	
4 conv	128	3x3	relu
5 conv	128	3x3	relu
6 maxpool		2x2	
7 conv	256	3x3	relu
8 conv	256	3x3	relu
9 conv	256	3x3	relu
10 maxpool		2x2	
11 conv	512	3x3	relu
12 conv	512	3x3	relu
13 conv	512	3x3	relu
14 maxpool		2x2	
15 conv	512	3x3	relu
16 conv	512	3x3	relu
17 conv	512	3x3	relu
18 maxpool		2x2	
19 flatten			
20 dense	128		relu
21 dropout	p = 0.50		
22 dense	16		softmax

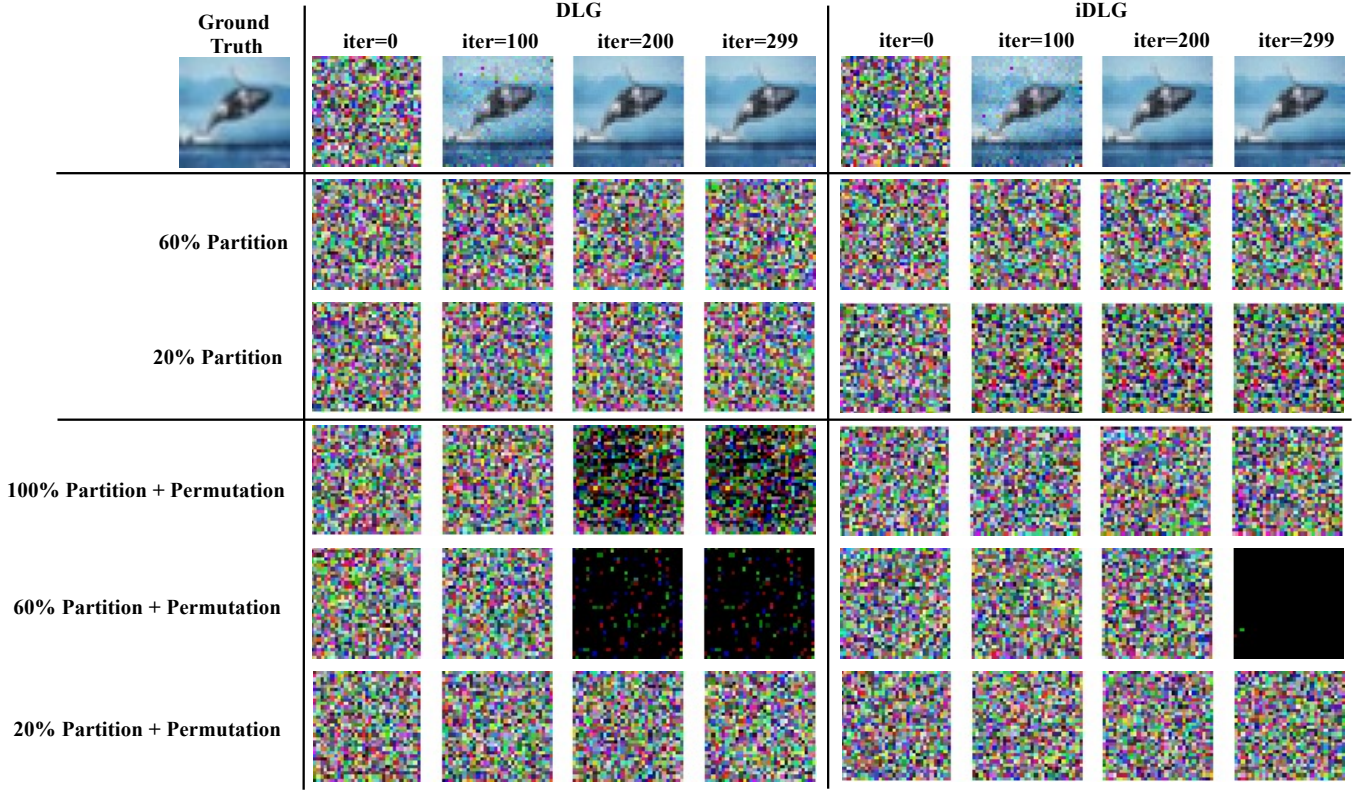


Figure 7: Reconstruction Examples of DLG and iDLG with Model Partitioning and Permutation

B RECONSTRUCTION EXAMPLES OF DLG/iDLG/IG

In Figure 7, we display the intermediate results of reconstructing an image using DLG and iDLG with different combinations of partitioning and permutation parameters. The first row of images shows the reconstruction results with the entire model updates, i.e., 100% partition, over 300 iterations. We use it as the baseline for comparison. The images at iteration 0 is the randomly initialized input. We observed that with the entire, unperturbed model update, DLG and iDLG can reconstruct most of the original image after 100 iterations. In the second and third row, we randomly kept 60%/20% of the model updates and provided them to the DLG and iDLG attacks. With only partial information, both attacks were unable to correctly minimize their respective cost function. Thus, the intermediate and final reconstructions do not contain any recognizable information related to the ground truth example. In the fourth through sixth rows, we randomly permuted the model updates

with 100%/60%/20% partitions respectively and ran the DLG and iDLG attacks. Similar to the previous results with partitioning only, the intermediate reconstructions do not contain any recognizable information related to the ground truth example. Of note is the fourth row of images, as they demonstrate that TRUDA’s permutation mechanism works even when only a single aggregator is present, which is traditionally used in FL.

In Figure 8, we display five *ImageNet* examples used in our IG reconstruction experiments. The first column shows the original images. The second column presents the reconstructed images (after 24,000 iterations) when the entire model updates (100% partition) were provided to the IG attack. These results are used as the baseline for comparison. In the third through seventh columns, we present the reconstructions with different combinations of partitioning and permutation enabled. Compared to the baseline, none of the reconstructions contain recognizable information related to the ground truth examples. Without the complete, unperturbed model updates, IG is unable to minimize its cost function.

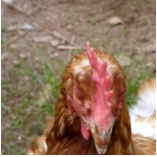

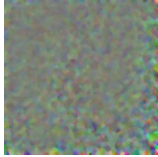
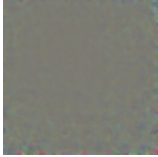
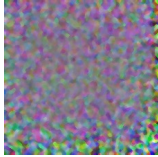
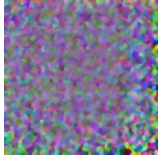
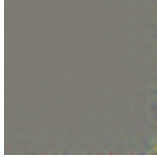


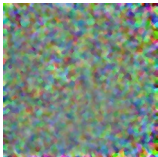

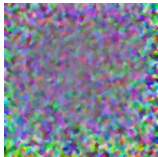

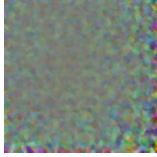



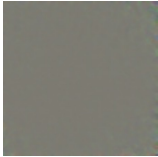
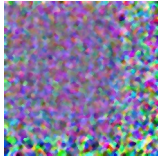
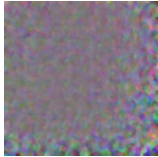



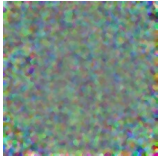

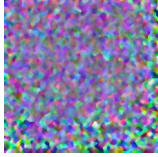
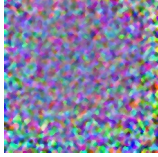
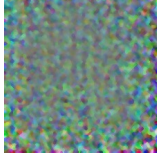


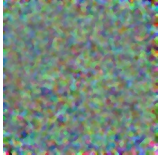
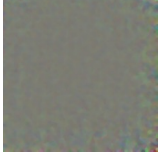
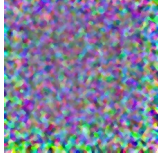
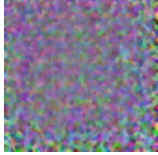
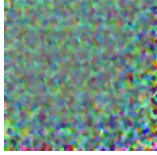
Ground Truth	100% Partition	60% Partition	20% Partition	100% Partition +Permutation	60% Partition +Permutation	20% Partition +Permutation
						
						
						
						
						

Figure 8: Reconstruction Examples of IG with Model Partitioning and Permutation